Intermetallics 154 (2023) 107825

Contents lists available at ScienceDirect

Intermetallics

journal homepage: www.elsevier.com/locate/intermet

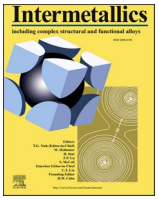

Investigation of mechanical properties of Al_3Zr intermetallics at room and elevated temperatures using nanoindentation

Abhinav Priyadarshi [a,*], Tungky Subroto [b], Jiri Nohava [c], Sedmak Pavel [c], Marcello Conte [c], Koulis Pericleous [d], Dmitry Eskin [b], Iakovos Tzanakis [a,e]

[a] Faculty of Technology, Design and Environment, Oxford Brookes University, Oxford, OX33 1HX, United Kingdom
[b] Brunel Centre for Advance Solidification Technology (BCAST), Brunel University London, Uxbridge, UB8 3PH, United Kingdom
[c] Anton Paar TriTec SA, Vernets 6, 2035, Corcelles, Switzerland
[d] Computational Science and Engineering Group (CSEG), Department of Mathematics, University of Greenwich, London, SE10 9LS, United Kingdom
[e] Department of Materials, University of Oxford, Oxford, OX1 3PH, United Kingdom

ARTICLE INFO

Keywords:
Al_3Zr intermetallic
Depth sensing indentation
Mechanical properties
Elastic modulus
Creep
High temperature

ABSTRACT

This work deals with the measurement of mechanical properties of single and polycrystalline Al_3Zr specimens from ambient to elevated temperatures using nano-indentation experiments. In this study, we employed three kinds of intermetallic specimens produced from Al_3Zr crystals chemically extracted from an Al-3 wt% Zr alloy. The properties such as elastic modulus and hardness were determined under quasistatic loading conditions. Constant multicycle indentation testing (MCT) was further performed using a Vickers indenter to understand the fatigue response of intermetallics at high load low cycle conditions. The results showed that hardness and elastic modulus of Al_3Zr intermetallics depended on the crystal structure/orientation, with polycrystalline samples showing higher elastic modulus than single crystal specimens at room temperature conditions. MCT experiments revealed that contact pressure of more than 7 GPa was needed to fracture a crack-free crystal under dynamic loading conditions. Consequently the properties of intermetallics at temperatures up to 700 °C were determined for the first time, using high-temperature nano-indentation technique. Elevated temperature measurements indicated that intermetallics had high creep resistance at low and intermediate temperatures, but exhibited significant plastic deformation and creep close to the melting point of pure aluminium.

1. Introduction

Aluminium based metal matrix composites (MMCs) have emerged as a highly desirable and promising advanced structural material that successfully meets the demands of a multitude of industrial applications, but more specifically in the automotive, aerospace and construction sectors [1–3]. In the last few decades, the use of transition metals (tri-aluminide (Al_3X) intermetallic compounds (IMCs) such as Al_3Zr and Al_3Ti) as reinforcements in Al alloys has attracted a lot of attention in developing high quality MMCs with advanced thermo-mechanical properties [4–8]. These primary intermetallic crystals, however, tend to have a needle or plate-like morphology with propensity to evolve into large particles that can adversely affect the mechanical properties of the alloy. Hence, their fragmentation or suitably changed morphology would be beneficial for the mechanical properties of the as-cast MMC. It has been also observed that the refined primary crystals can nucleate Al grains, and therefore, further fragmenting them during the growth phase within the solidifying melt can be highly beneficial [9]. To this end, our team pioneered the microstructural refinement of aluminium alloy structures [10–13] through the mechanism of cavitation-induced fragmentation of primary phases within the high-temperature melt by employing ultrasonic treatment and novel acoustic measurement techniques, thereby controlling [14,15] and increasing the nucleation potency of such refined crystals [16]. Recently, efforts have also been made to understand the mechanism of fragmentation of primary intermetallics induced by cavitation [11,17–19]. However, lack of information related to mechanical properties such as hardness (H), Young's (elastic) modulus (E), and fracture toughness (K_c) of these IMCs especially at high temperatures, prevented an accurate analysis and further numerical modelling and optimisation of this process. Hence, measuring the mechanical properties of primary intermetallics such as Al_3Zr – that provide thermal stability and improve strength of alloys by simultaneously

* Corresponding author.
E-mail address: apriyadarshi@brookes.ac.uk (A. Priyadarshi).

https://doi.org/10.1016/j.intermet.2023.107825
Received 4 November 2022; Received in revised form 22 December 2022; Accepted 2 January 2023
Available online 6 January 2023

eliminating the use of costly grain refiners in aluminium alloys at elevated temperatures is of high technological importance.

Depth sensing indentation (DSI) is an established instrumented nanoindentation technique that primarily operates at nanometre resolution with sub-micron depth ranges under nano/milli-Newton load conditions [20,21]. It is considered a very reliable tool for probing physical-mechanical properties, mainly elastic modulus and hardness, at finitely small length scales through the continuous capturing of indentation force and the resulting indentation depth [22]. Different experimental (ultrasonic acoustic wave, microhardness indentation) and theoretical (first principles method) approaches have previously been undertaken to evaluate the physical properties of Al_3Zr crystals at room temperature (RT) [23–32]. However, to the best of our knowledge, only one study has been conducted in the past that discusses the effect of temperature on the microhardness of Al_3Zr and other high-temperature binary IMCs [25]. Though, the variation of moduli with temperature was not addressed in this work that would have allowed better understanding of the mechanical behaviour with respect to temperature. High temperature (HT) DSI measurements can help fill this existing gap in the literature.

The current work focuses on the determination of mechanical properties of single crystal Al_3Zr IMCs at elevated temperatures (from RT up to 700 °C). Prior to the HT measurements, hardness and the elastic modulus of three differently prepared intermetallic specimens i.e. Al_3Zr phase in Al matrix (reference sample for RT experiments), polycrystalline Al_3Zr and embedded single Al_3Zr crystals in cement matrix (especially produced for HT measurements) were compared and analysed to check for any property variation at RT, and whether the surrounding matrix and intermetallic orientation had any influence on the nanoindentation measurements. The Al_3Zr phase in Al matrix was also subjected to constant multicycle indentation testing (MCT) to understand the fatigue behaviour of the IMCs under different indentation loads at RT. The primary purpose of this research work is to measure the mechanical properties of Al_3Zr IMCs (with novel and bespoke sample preparation method) using a standard nanoindenter equipment at elevated operating temperatures that can feed into our advanced numerical models and further assist optimisation of microstructural refinement process for ultrasonically treated Al alloy melts. However, taking into consideration the experimental challenges faced during the preparation of intermetallic specimens in terms of production, extraction and their mounting (especially for polycrystalline Al_3Zr and embedded single Al_3Zr crystals in a cement matrix), we have confined our findings only under specific loading conditions that simulate the high pressure and temperature field environments encountered during the melt processing experiments.

Results demonstrated for the first-time that the hardness and elastic modulus of Al_3Zr IMCs abruptly decrease while creep tends to increase at approximately half-melting temperature of the intermetallic.

2. Materials and methods

2.1. Sample preparation

Three types of intermetallic specimens were used for the mechanical property measurements i.e., 1) single Al_3Zr crystals in Al matrix, 2) arc-melted pure polycrystalline Al_3Zr for room temperature measurements, and 3) embedded single Al_3Zr crystals in a cement matrix for high temperature measurements. For easy referencing, we will refer to the studied specimens as Sample 1 (Al_3Zr in Al matrix), Sample 2 (polycrystalline Al_3Zr) and Sample 3 (Al_3Zr embedded in cement matrix). These different intermetallic specimens were prepared in order to check for any variation in the measurements at RT between the single (Sample 1 and Sample 3) and polycrystalline (Sample 2) specimens and to compare if the cement matrix specimen qualifies for the high temperature measurements. Except for Sample 1, the other two specimens were produced from the extracted primary crystals. The crystal extraction process using NaOH has been discussed elsewhere [17].

The preparation method of Sample 1 has been discussed elsewhere [17,18]. For preparing Sample 2, 3–4 g of extracted Al_3Zr flakes were arc melted using a non-consumable electrode arc-melting device to produce a 'T' shaped rod of length 10–12 mm and approximately 1.5 mm thick in order to comply with the testing requirements (see section 2.2). Due to the extreme brittleness of intermetallics, the sample was then embedded and moulded using a low-melting point Sn-57 wt% Bi alloy to enable grinding and polishing. After polishing, the Sn-57 wt% Bi alloy was melted at 139 °C and the extracted polycrystalline sample was used for nanoindentation experiments. For preparing Sample 3, the extracted primary Al_3Zr crystals of dimension approximately 2 ± 1 (L) $\times$ 3 ± 2 (W) mm and thickness of 60–70 μm were distributed uniformly facing their wider plane on the surface of a glass slide (coated with thin layer of oil/grease). A high temperature cement/ceramic adhesive paste (Pelco High Performance Ceramic Adhesive, Ted Pella, Inc, USA) was then poured onto the glass slide and was confined within the circular ring of 25-mm diameter. The adhesive paste was then carefully covered by another glass slide over the top to make the surfaces flat at both ends. The thickness of the sample was kept close to 5 mm to limit the potential thermal shock and the flatness between the two faces was adjusted to be within 20 μm. The adhesive was subsequently air dried and solidified at room temperature. The dried cement adhesive embedded with intermetallic crystals was then removed from the slides and cured at 93 °C for approximately 2 h (following the manufacturer instructions). This was deliberately done to achieve good mechanical properties of the solidified ceramic matrix at elevated temperatures. The samples were then mechanically polished to a mirror finish with average surface roughness (R_a) maintained around 0.4 μm for both sample faces before using them for the nanoindentation experiments. Fig. 1a represents the concise flow chart of the specimen preparation for sample 2 and 3 and Fig. 1b-d shows the optical micrographs of the three intermetallic specimens used in this study. It should be noted that the Al_3Zr crystals (enclosed in red region) in Sample 1 are facing its edges unlike Sample 3.

2.2. Nanoindentation experimental setup

An ultra-high temperature nano-indentation setup (UNHT HTV, Anton Paar, Switzerland) working on a principle of active surface referencing and infrared heating of the sample was used to measure the mechanical properties of Al_3Zr intermetallic specimens at both RT and HT. This measurement principle employs measuring and referencing axes, each with their own means of controlling the applied load. The active reference principle ensures excellent thermal stability of the instrument even at temperatures up to 700 °C without the need of correction of the thermal drift and eliminates to a great extent the need to correct the frame compliance. Additional details regarding the instrumentation setup and configuration are provided elsewhere [33].

For RT measurements, successive indentations were performed on all three specimens with continuous loading and unloading speeds of 20 mN/min and a dwell time of 5 s, using a Berkovich diamond indenter. The load–displacement characteristics were acquired with a linear quasistatic loading of 10 mN and an acquisition frequency of 10 Hz. Sample 1 was further subjected to MCT mode in order to measure the low cycle fatigue response as we have previously seen that intermetallics under the action of cavitation bubbles break in a low cycle fatigue mode [17–19]. For MCT measurements, 100 cyclic indentations were performed using a Vickers indenter with maximum and minimum loads of 1 and 0.5 N, and 5 and 3 N, respectively, at loading and unloading durations of 10 s, dwell time of 2 s and acquisition rate of 50 Hz.

HT nanoindentation measurements were carried out to specifically determine the hardness and elastic modulus of primary intermetallics from RT up to 700 °C at intervals of 50 °C. The choice of a 50 °C interval was a compromise between the resolution and duration of the measurements. To the best of our knowledge, this is the first HT nanoindentation study for this type of IMCs. Sample 3 was used for these

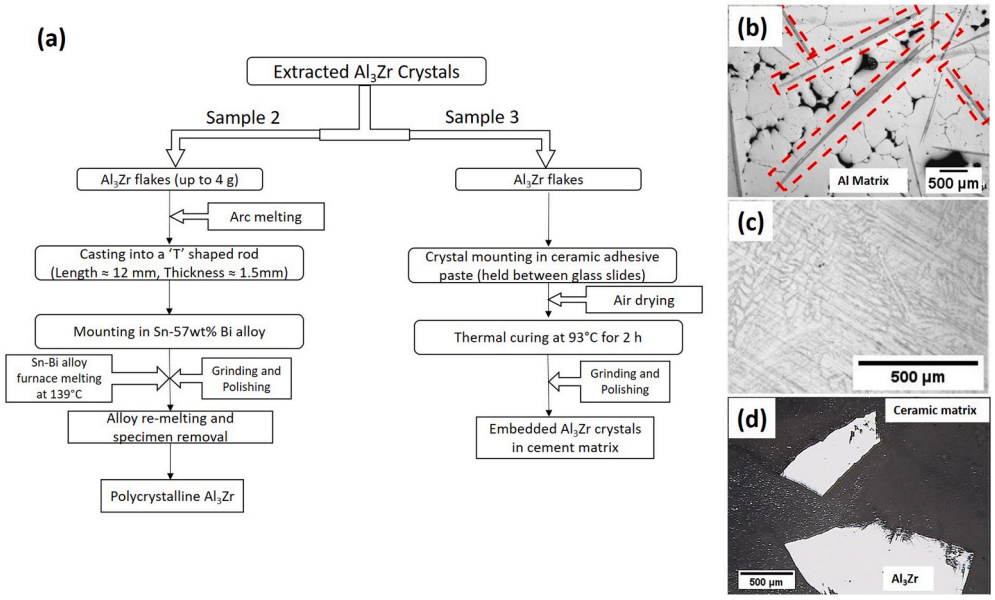

Fig. 1. (a) Flow chart of intermetallic specimen preparation for sample 2 and 3. Representative optical micrographs of (a) Al_3Zr crystals in the Al matrix, (Sample 1); (b) polycrystalline Al_3Zr solidified as dendritic grains (Sample 2); and (c) Al_3Zr embedded in the cement matrix (Sample 3).

measurements. To avoid surface oxidation of the specimen, especially at elevated temperatures, the indentations were performed in vacuum (10^{-6} mbar) with loading and unloading speeds of 120 mN/min and dwell period of 2 s. The load-displacement profiles were obtained with a maximum load of 10 mN with an acquisition rate of 400 Hz. At least 5 indents were carried out for each measurement condition to achieve statistically reliable data.

3. Results and discussion

3.1. Room temperature measurements

Mechanical properties (E, H and K_c) of Sample 1 at RT have been reported in our previous work [17,34]. In this study, we went a step further and first compared the mechanical properties of three different intermetallic specimens and analysed the effect of quasistatic indentation loading on the hardness and elastic modulus values at ambient conditions using Oliver and Pharr (O&P) method. Sample 1 was additionally subjected to dynamic indentation loading, where we looked into the fatigue characteristic of these intermetallics to assist in understanding the fragmentation mechanism upon ultrasonic treatment of aluminium alloys and to provide important input parameters for accurate numerical modelling of the process [35].

Fig. 2a shows the typical indentation load (P)-displacement (h) curves and Fig. 2 (b and c) shows the bar chart that represents the H and E values of the examined samples, respectively. All the indentations were performed on unetched samples.

It is apparent from Fig. 2a that both single (Samples 1 and 3) and polycrystalline (Sample 2) specimens show elastic-plastic response. The load-displacement curves for all the specimens display an almost similar shape differing only in the maximum (h_{max}) and final (h_f) indentation depth, highlighting the resistance of the indenter penetration into the bulk specimens. For a fixed maximum indentation load (P_{max}), the intermetallic types can be classified based on h_{max}. Under the P_{max} of 10

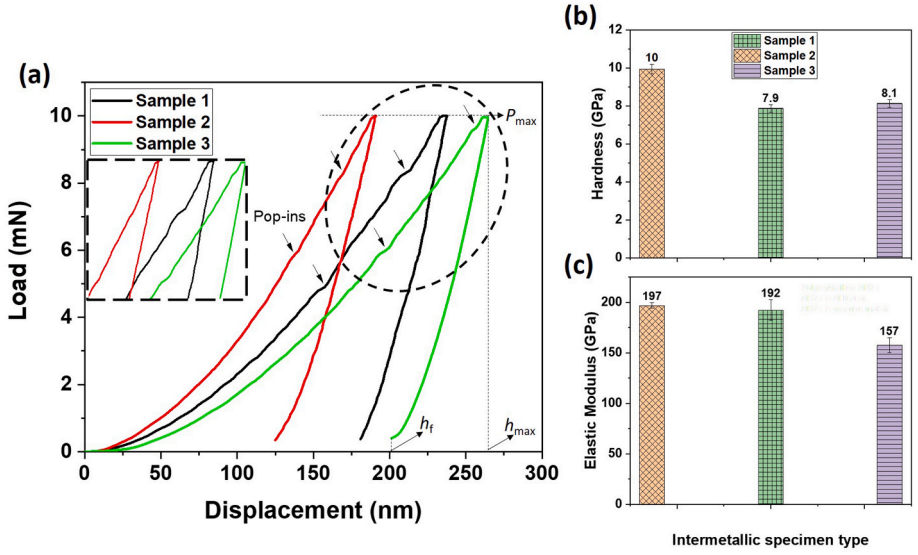

Fig. 2. Comparison of nanoindentation response of different intermetallic specimens in terms of (a) Load-displacement curve, (b) indentation hardness, and (c) indentation modulus.

mN, h_{max} was found to be different for all the samples and varied between 214 nm for Sample 2 and 252 nm for Sample 3 with Sample 1 having h_{max} close to 236 nm. After the elastic recovery during unloading, variation in h_f was between 152 nm for Sample 2 and 188 nm for Sample 3 with Sample 1 having h_f around 181 nm. The indentation curves exhibited approximately similar amount of elastic recovery during unloading, i.e. ~23% for Sample 1, ~29% for Sample 2 and about 26% for Sample 3. It is interesting to note that the nanoindentation curves for all the specimens show some arbitrary discontinuities specifically on the loading curve. The initial discontinuities (displacement burst) present in the form of 'pop-ins' (see arrows on Fig. 2a) can primarily be attributed to the nucleation of dislocations during loading by the indenter [21]. Other possible reasons for these discontinuities can be linked to the strain/slip transfer at the interfacial plane and grain boundary (GB) regions (for Sample 2), where dislocations penetrate and transfer into the subsequent layers/interface [36,37]. The similar observed displacement burst has also been classified as 'initial pop-ins' or 'GB pop-ins' elsewhere [37]. Britton et al. [37] reported that the 'initial pop-in' is generally due to activation and multiplication of dislocations and occurs at shallower indentation depths, while 'GB pop-in' is observed at larger depths and is linked to the interstitial pinning of dislocations at or close to the interface/boundary. It is important to note here that extracted single crystal Al_3Zr intermetallics are layered materials and exhibit tabular and faceted structure along the habit planes by virtue of their growth morphology [18,38,39]. While the pop-ins in Fig. 2a are less noticeable in Sample 2, they are much more discernible and apparent in the case of single crystal IMC specimens, i.e. Sample 1 and Sample 3, indicating the effect of tabular/layered structure during indenter loading. Any other minor discontinuities may also be a result of contaminating surface layers, vibrations present in the measuring device or the feedback cycle occurring during indentation testing.

For the evaluation of E and H from P-h curves using O&P method, another important parameter of measurement is the contact indentation depth (h_c) that can be estimated using the expression suggested by O&P, $h_c = h_{max} - \varepsilon (P_{max}/S)$, where S is the contact stiffness (slope of unloading curve) and ε is the indenter constant. This expression turns out to be approximately equivalent to the average of h_{max} and h_f. However, with the advancement in the measurement techniques, the contact depth can also be accurately measured using the software provided with UNHT device. From Fig. 2b, it can be seen that Sample 2 offers the largest resistance to the localised elasto-plastic deformation (hardness) preferentially due to the presence of grain boundaries that obstruct dislocation/crack motion nucleated during indenter loading, followed by Sample 3 and Sample 1, which have almost similar values. It is a well-accepted fact that dislocations formed during material deformation (indentation) can contribute to the enhancement of their mechanical properties owing to the phenomenon known as dislocation hardening [40]. In the case of a polycrystalline material, the interaction between dislocations and the grain boundaries is much more complex with smaller plastic deformation than in single crystals [41]. The accommodation of lattice dislocations further becomes difficult in smaller size crystallites and thus any local non-uniformity in the crystal lattice of the IMCs can further impede the movement of dislocations resulting in enhanced mechanical properties as previously reported by Bi et al. [42]. The P-h curve for Sample 3 is also a good analogue to Sample 1, which makes them suitable for high-temperature measurements. However, it should be noted that crystal orientation may play a role. In the case of Sample 1, the crystal is penetrated at its edges (a cross-section as it is the most common orientation that one can get when sectioning a 3D sample), whereas in the case of Sample 3, the crystals were deliberately placed facing their flat (wider) plane. Therefore, some discrepancy in the measuring values may be expected especially with the flat plane orientation, where the occurrence of internal/substrate defects is more likely (larger area). The differences in the measured hardness of the intermetallic specimens (although not significant) are also obvious from the variation of h_{max} as observed in Fig. 2a. Fig. 2c shows the measured elastic modulus of different intermetallic specimens. Sample 1 and Sample 2 showed similar E values in contrast to Sample 3 that exhibited the lowest modulus. This difference can be explained by the fact that the indentation modulus is derived from the observed contact area and the parameter S that is critical in its calculation and is smaller in case of Sample 3. It should be noted that the hardness is gauged from the indenter displacement, giving rise to plastic deformation, whereas the modulus is dependent mainly on the elastic stress fields. In addition, the large drop in the modulus value of Sample 3 might also be explained in terms of crystal orientation (edge vs. plane) used for indentation and the effect of the extended plastic zone into the surrounding matrix. This elastic anisotropy is believed to be strongly related to the crystallographic orientation of the material being tested [23,43]. However, the detailed examination of this effect is outside the scope of this work. Based on these observations, we can say that single (Sample 3) and polycrystalline (Sample 2) intermetallics show similar material behaviour without large differences in the mechanical properties, which means that indentations are successfully localised in tiny areas unaffected by grain boundaries or other defects. However, the variation in elastic modulus for Sample 3 can be attributed to high surface to (hidden) defect ratio. Moreover, the smaller thickness of the specimen with potentially formed crack networks makes the indentation measurement prone to interaction with hidden defects underneath the measured crystal.

Chen et al. [44] pointed out another interesting feature that could be correlated with the elastic modulus, which is the temperature of formation of these intermetallic phases. Based on the thermodynamic modelling, it is predicted that intermetallic phases with a higher modulus are actually formed at a higher temperature and vice versa. The higher the formation temperature, the larger the required enthalpy. The reason for this correlation lies in the notion that a higher heat of formation accounts for a tighter and stronger atomic bonding, thus resulting in a higher modulus [45]. Such analysis is, however, beyond the scope of this work and is only presented as an overview of nanoindentation measurements.

In order to characterise the fatigue behaviour of the intermetallic phase, Sample 1 was further subjected to MCT experiments at the maximum and minimum loads of 1, 5 N and 0.5, 3 N, respectively, for 100 cycles simulating the conditions of very low-cycle fatigue. Fig. 3a shows the load-displacement curves and the corresponding indentation marks (Fig. 3(b and c)) formed within the intermetallic phase. It can be seen that the indentation performed at 1 N maximum load did not produce any cracks (Fig. 3b) within 100 cycles and the IMC only undergoes elasto-plastic deformation. Whereas the indentations performed at 5 N maximum loads showed the presence of multiple pop-in and cracking events (see Fig. 3a) during the initial loading itself. The appearance of pop-ins in the P-h curve maybe attributed to either nucleation/slipping of dislocations beneath the indenter tip [46] or instantaneous fracturing [47] of intermetallics (indicated by a sudden increase in the penetration depth [48]) as seen in Fig. 3 (d), which shows the formation of cracks originating at the sides and corners of the indent. Other than widely attributed mechanism of homogeneous dislocation nucleation to explain the pop-ins, there has also been experimental and theoretical evidence, where discontinuous steps can be generated through heterogeneous dislocation nucleation under the presence of surface steps and/or ledges in the material [49,50]. The presence of such surface layers contributes to the pop-in events in a similar fashion as to those recognised during the GB effect on nanoindentation [36,37] as discussed earlier. A zoomed-in figure of the indentation mark obtained at 5 N load (Fig. 3d) clearly shows the occurrence of steps/layers within the Al_3Zr intermetallic owing to their growth morphology thereby confirming their role in generating pop-ins. When the indenter is in close proximity of these steps/layers, the load required to create dislocations diminishes, thus their nucleation becomes easier [49]. Moreover, the presence of pop-ins could also indicate shifting of intermetallic behaviour from elasto-plastic to plastic deformation [51]. Interestingly, the

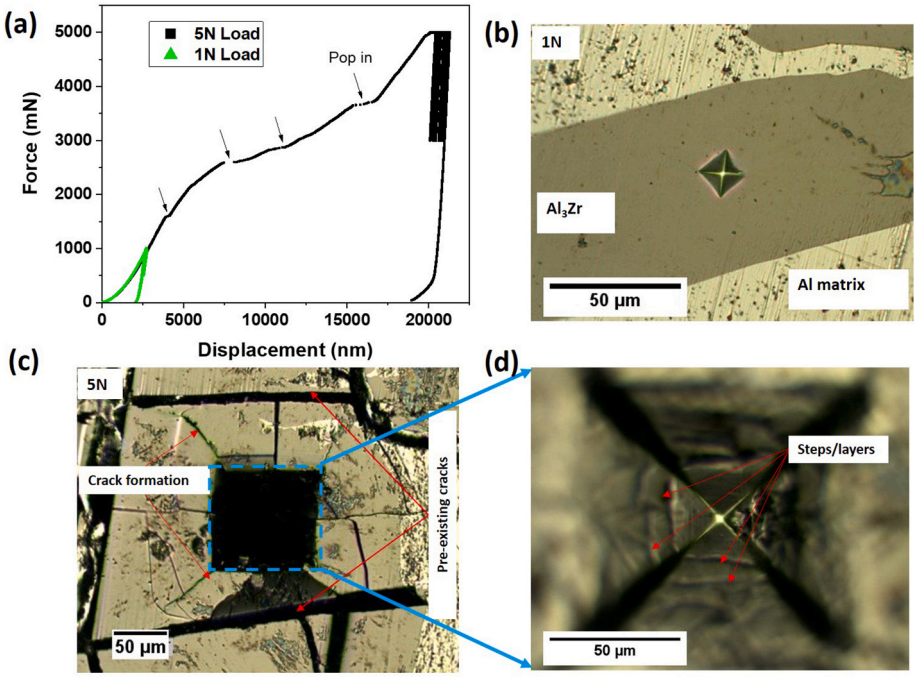

Fig. 3. Constant multicycle indentation testing showing (a) *P-h* curves and corresponding indentation marks formed at maximum applied load of (b) 1 N and (c) 5 N after 100 cycles with (d) zoomed-in image of the indentation mark in (c).

Al_3Zr intermetallic exhibited multiple instance (onset) of cracking events during loading up to 5 N (see arrow in Fig. 3a) while there was no sign of any fracture during loading when indented with a 1 N load. This can be attributed to the presence of pre-existing cracks within the intermetallic particle used for indentation (see Fig. 3c) that may have formed during solidification of the base Al-3%Zr alloy due to thermal contraction stresses.

In this study, it was not possible to detect the crack propagation in the Al_3Zr phase at the maximum load of 5 N as the intermetallic fractured well before the initiation of cyclic loading. Therefore, to understand the fatigue response, we plotted the contact depth of the indenter displacement as a function of indentation cycles. Fig. 4 shows these data for 1 and 5 N loading cases. Note the different scales of the y-axes for different loads have been adjusted such that the changes in contact depth can be discernible and comparable. For the 1 N load, the indentation depth decreased by almost 60 nm during 100 cycles. While in case of the 5 N loads, the indentation depth increased by about 900 nm. The decrease in the indentation depth at the 1 N load could likely be due to stiffening of material during cycles of loading and partial unloading caused by the multiplication of dislocations and their mutual entanglement/trapping [52]. However, these MCT measurements did not show any evidence of the development of fatigue induced cracks. Instead, the increase in contact depth as observed for the 5 N loading could just be the propagation of cracks generated during quasistatic

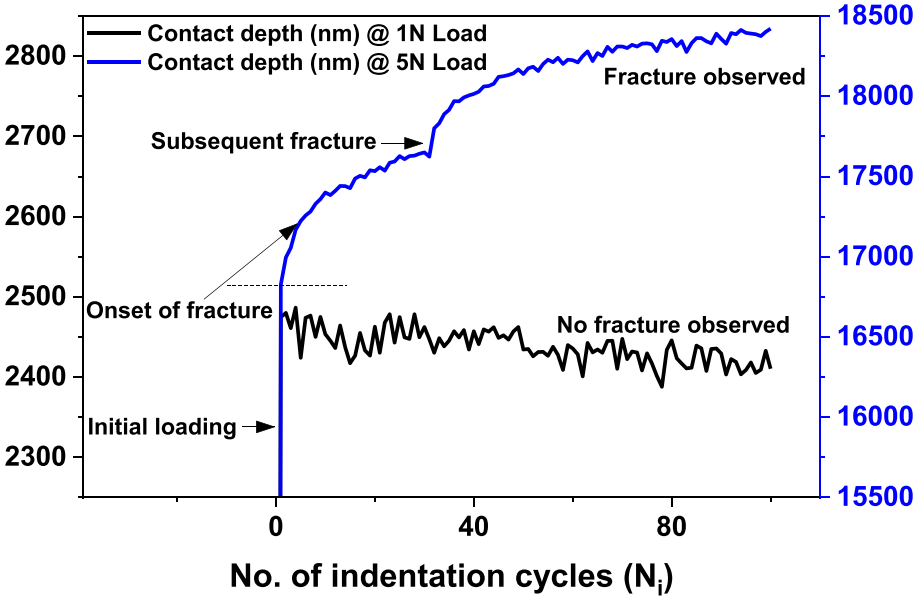

Fig. 4. Variation of contact depth of the indenter as a function of indentation cycles for maximum loads of 1 and 5 N, showing the onset and subsequent fracture observed during loading.

loading as seen in Fig. 3a, i.e., the point of subsequent fracture (indicated by the sudden increase in contact depth) under 5 N load as shown in Fig. 4 that formed during the initial loading period as discussed above. For 1 N loading (Fig. 3a and b), however, no fracture was observed during loading and unloading cycle meaning that the intermetallic must have sustained the generated indentation stress (contact pressure) without initiation of fatigue cracks. Upon the formation of a fully developed plastic zone after unloading of the indenter (see Fig. 3b), the contact pressure becomes equivalent to the indentation hardness of the specimen, which was found out to be approximately 7 ± 0.2 GPa. It is important to note here that the mean contact pressure can be constant irrespective of the applied load once the yield stress is exceeded. However, higher loads lead to higher strains and material displacement near the indent, which further facilitates the initiation of fracture. That is why the cracks are observed at a higher load (5 N) rather than at a lower load (1 N). Moreover, it has also been reported that in materials containing small number of defects, e.g., those without any micro/nano cracks in highly brittle materials, deformation is based on defects formed during indentation; and the contact pressure in such cases can increase to values equivalent to the theoretical strength in a perfect single crystal [53]. However, the mean pressure can further drop once the dislocation nucleates upon increasing the indentation load (observed in the form of pop-ins). From Fig. 3a, it can be seen that for 1-N loading, there are no visible pop-ins present but for 5-N loading (with pre-existing cracks formed during solidification due to thermal contraction stresses), there is generation of multiple pop-ins attributed to the development of further cracking/chipping events during indentation. Based on the MCT measurements, it can be deduced that these brittle intermetallics in the case they are free of pre-existing cracks, can only be fractured if the applied contact pressure (hardness) goes beyond 7 GPa (1 N load) and large strains near the indent are created. However, in reality and during cavitation-induced fragmentation, the situation is more complicated. The fracture toughness of such IMCs is low (~1 MPa$\sqrt{m}$) [17] and the observed fracture due to liquid jets [54] and emitted shock waves [55] from imploding cavitation bubbles happens under much lower impact pressures ranging from 0.4 to 2 MPa [17,18], indicating the presence of multiple defects. Similar behaviour can be seen in the case of 5 N load due to propensity of pre-existing cracks formation/accumulation across the substrate.

3.2. High-temperature measurements

Following the evaluation and comparison of mechanical properties, i.e., *E* and *H* using quasistatic DSI experiments for different intermetallic specimens at ambient conditions, Sample 3 was then subjected to elevated temperature measurements for determining the effect of temperature on the mechanical properties estimated at up to 700 °C at 50 °C intervals.

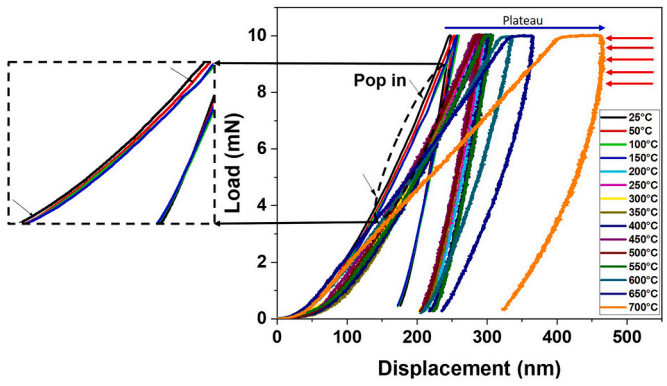

Fig. 5. Typical load-displacement curves for Al_3Zr crystals embedded in ceramic matrix measured from RT up to 700 °C.

Fig. 5 shows the comparison of typical *P-h* curves for the specimens measured from RT to 700 °C. The dwell period of 2 s was kept constant for all the indentation experiments performed at elevated temperatures. As expected, the maximum indentation depth was almost doubled, with the increase in operating temperature from RT to 700 °C and measured to be 248 nm and 462 nm, respectively. Between two consecutive indentation temperatures, the increase in the indenter depth was less than 10% except at 650 °C and 700 °C where this increased up to 22% indicating that the material became softer at such high temperatures. As the temperature was increased, the load displacement curves started to exhibit a steady plateau region during the dwell interval with maximum indentation load (indicated by blue arrow in Fig. 5). This can be possibly ascribed to the plastic deformation and development of creep, indicating that Al_3Zr crystals undergo creep at relatively high temperatures (~600–700 °C). However, with a limited dwell period for indentations performed at such temperatures, an intermetallic fails to undergo full plastic relaxation in the creep regime in comparison to low (25–200 °C) and intermediate temperature (200–550 °C) ranges, which is noticeable in the form of convex bending (indicated with red arrows in Fig. 5) during unloading of the indenter similar to observations made for intermetallic phases such as Al_7Cu_4Ni and Al_2Cu at 350 °C [56]. Thus, the determination of elastic modulus values at such a high temperature should be handled with extreme care. Moreover, at this temperature, contribution from the elastic energy to the material deformation is also very small. With the increasing temperature especially in the intermediate and high range, the amount of elastic recovery during indentation unloading also decreases, which indicates larger portion of plastic deformation.

Results showed the appearance of discontinuities within the indentation loading and unloading curve at elevated temperatures (200–700 °C) in form of serrations. Additionally, only some of indentation curves up to 150 °C showed the presence of discernible small pop-ins (see black arrows in Fig. 5) during loading of the indenter indicating plastic yield of the material at nanoscale that could be related to dislocation events emerging underneath the indenter tip. The sudden displacement of indenter (pop-ins) typically occurs at indentation stress, which is equivalent to the material maximum shear strength that triggers the nucleation of dislocations followed by their propagation. At relatively low temperatures, the movement and interaction of the formed dislocations leads to strain hardening in crystalline materials [57]. Increasing temperature can further shift the plastic yield indentation loads, which are primarily driven by the dislocation nucleation kinetics at homologous temperature of crystalline materials. It is also known that exposure to elevated temperatures facilitates dislocation movement and re-arrangement, and is accompanied by the significant reduction in the dislocation density [56]. This instability of plastic deformation caused by the counterbalancing between the dislocation induced hardening/stiffening and dislocation reduction/recovery process characterises the creep behaviour at higher operating temperatures (~0.4–0.5 T_m, where T_m is the melting temperature in K). Gupta et al. [58] reported that Al_3Zr crystals are highly stable at a creep test temperature of 330 °C (about 0.38 T_m) because of their high melting point, i.e. approximately 1580 °C. Moreover, a homogeneous creep deformation in materials is usually observed at temperatures that are above the half-melting-point value, which is around 654 °C (927 K) for these crystals. Therefore, the dislocation events are mainly associated with the discontinuities during indentation loading, observed as serrations in the form of pop-ins, whereas the homogeneous plastic deformation tends to appear in the form of a continuous shift (plateau region in Fig. 5), which is affected by the free volume redistribution during indenter penetration [56].

Fig. 6 shows the variation of mechanical properties i.e. *E* and *H* with temperature up to 700 °C. As expected, the elastic modulus and hardness decrease with increasing temperature. With a slight increase in temperature up to 100 °C above RT, the modulus decreased by almost 23% whereas hardness decreased by approximately 18%. The biggest drop in

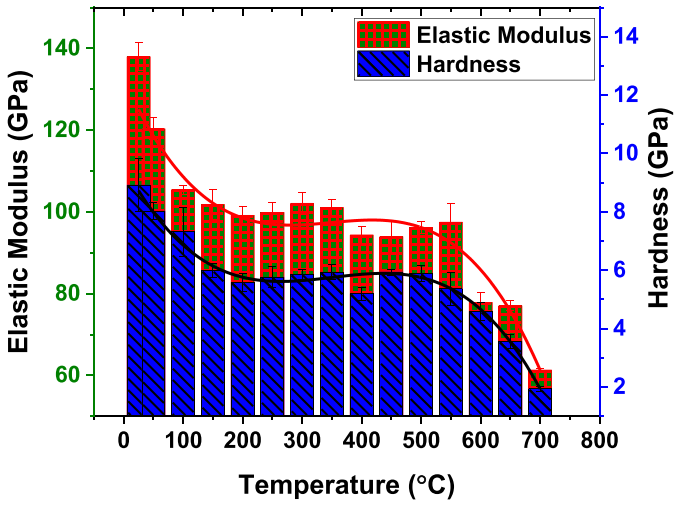

Fig. 6. Variation of elastic modulus and hardness as a function of indentation temperature for Al_3Zr intermetallics.

hardness of about 46% was observed between 650 °C and 700 °C, whereas elastic modulus dropped by 20% indicating creep initiation of the intermetallic. Overall, both the hardness and elastic modulus decreased by almost 78% and 55%, respectively, from RT to 700 °C. At RT, hardness is governed by the evolution of dislocation network, while at HT the change in the indentation hardness has been correlated to creep and plastic flow behaviour [57]. As seen from Fig. 5, the higher the temperature, the lesser the elastic recovery during the unloading of the indenter as seen from h_f. For example, the elastic recovery decreased by approximately 29% at RT to 25% at 700 °C as seen from the percentage change in h_{max} and h_f. This partial elastic recovery can greatly influence not only the maximum displacement of the indenter but also slope of the curve during initial unloading that is utilised for evaluating parameters such as E and S as seen from the convex bending at 700 °C. The incomplete recovery can cause the gradient of the unloading curve to reach almost 90° leading to imprecise fitting using a power law function as per O&P model, which can eventually result in high inaccuracies in the measured modulus values. Hardness, on the other hand, remains more or less unaffected in such cases as its evaluation takes into consideration h_c, which relies less on the slope S but more on the maximum indenter depth (h_{max}). For example, assuming the case of 90° slope in the beginning of the unloading curve, the term 'ε (P_{max}/S)' will become negligible in the expression, $h_c = h_{max} - \varepsilon$ (P_{max}/S) and thus will only depend on h_{max} and not the contact stiffness S. The modulus can also be affected by the surface roughness of the specimen if the indentation is made in a relatively rough region, which can be very sensitive at HT [59]. In addition, the loading frame compliance can significantly increase during elevated temperature conditions leading to an increase in modulus value.

Both hardness and elastic modulus exhibited two regions of large drop in values with increasing temperature, one at low temperature (50–200 °C) and then at relatively high temperature (500–700 °C) as shown in Fig. 6 indicating the gradual softening of the material. Similar behaviour of this intermetallic in terms of microhardness variation with temperature has been previously reported by Fleischer et al. [25] who observed that the Al_3Zr compound is still susceptible to cracking until ~750 °C. The temperature dependent properties of intermetallics can also be understood in terms of the deformation energy produced during indentation. Since the hardness of the material is related to a combination of various factors such as yield strength, strain hardening coefficient and resulting plastic strain of the material, the most efficient way of evaluating the deformation energy is by using the ratios, H/E and H^3/E^2 that take into account the creep effects. The H/E ratio points towards the cracking resistance to elastic failure indicative of the toughness characteristics and H^3/E^2 defines the plastic deformation resistance during a plane contact [60]. Fig. 7 displays the variation of H/E and H^3/E^2 with an increasing operating temperature. It is clear from the figure that both ratios decrease non-monotonically with temperature. At the same time, the plasticity index i.e., the ratio of plastic work (W_p) to total indentation work (W_t) increases non-monotonically with temperature, most notably above 600 °C and is inversely related to H/E [61]. For Al_3Zr intermetallics, it can be seen that H/E is around 0.06 at RT, which means that the material is very brittle within the elastic limit, which agrees well with the low fracture toughness value at RT and previous observations of shuttered crystals [17,18,34]. On the other hand, H^3/E^2 is almost zero at an elevated temperature (close to 700 °C) with plasticity index of almost 80% indicative of its low creep resistance.

4. Conclusions

In this study, mechanical behaviour of Al_3Zr intermetallics was studied using the depth sensing indentation technique. The experiments were performed using quasistatic and multicycle indentation loading to evaluate the mechanical properties of three differently produced Al_3Zr intermetallic specimens. High temperature nanoindentation was also performed to determine the variation of hardness and elastic modulus with temperature. The results showed that.

1. The polycrystalline Al_3Zr sample exhibits about 24% and 22% higher hardness than the Al_3Zr phase in the Al matrix and the extracted crystals embedded in the cement matrix, respectively, possibly due to the nucleation of dislocations indicated by the 'pop-in' events observed during indenter loading and obstruction of their motion by the grain boundaries.
2. Multicycle indentation experiments show that the defect-free Al_3Zr intermetallic can sustain a contact pressure of almost 7 GPa before failing under low external loading (1 N) when large strains near the indent are created.
3. High temperature nanoindentation of Al_3Zr crystals shows that both hardness and elastic modulus decrease with temperature between RT and 700 °C by 78% and 55%, respectively. This intermetallic offers strong creep resistance at low (RT to 200 °C) and intermediate (200 °C–500 °C) temperatures.
4. At temperatures close to the melting point of pure Al, Al_3Zr intermetallics undergo large plastic deformation indicative of high atomic disorder making the plastic flow inherently unstable.

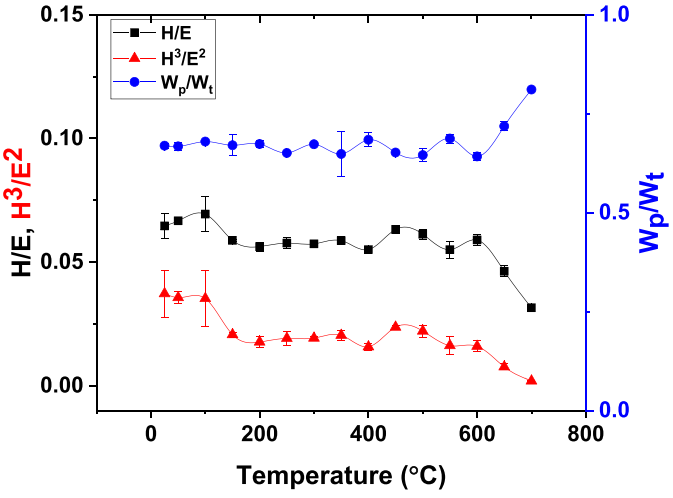

Fig. 7. Variation of elastic strain to failure, plastic deformation resistance and plasticity index with indentation temperature of primary Al_3Zr intermetallic.

CRediT author statement

Abhinav Priyadarshi: Conceptualization, Methodology, Data Curation, Software, Validation, Formal analysis, Investigation, Resources, Writing - original draft, Writing - review & editing. **Tungky Subroto:** Methodology, Investigation, Resources. **Jiri Nohava**: Formal analysis, Investigation, Writing - review & editing. **Sedmak Pavel:** Formal analysis, Investigation, Writing - review & editing. **Marcello Conte**: Formal analysis, Investigation. **Koulis Pericleous:** Writing - review & editing, Supervision, Funding acquisition. **Dmitry Eskin:** Writing - review & editing, Resources, Supervision, Funding acquisition. **Iakovos Tzanakis:** Writing - review & editing, Supervision, Funding acquisition.

Declaration of competing interest

The authors declare that they have no known competing financial interests or personal relationships that could have appeared to influence the work reported in this paper.

Data availability

Data will be made available on request.

Acknowledgements

This work was financially sponsored by the UltraMelt2 project with grants EP/R011001/1, EP/R011095/1 and EP/R011044/1 funded by the UK Engineering and Physical Sciences Research Council (EPSRC). Authors greatly acknowledge the help received from Mr. Qing in preparing the arc-melted specimens.

References

[1] F. Nturanabo, L. Masu, J. Baptist Kirabira, Novel applications of aluminium metal matrix composites, alum. Alloy, Composer (2020), https://doi.org/10.5772/INTECHOPEN.86225.
[2] P. Samal, P.R. Vundavilli, A. Meher, M.M. Mahapatra, Recent progress in aluminum metal matrix composites: a review on processing, mechanical and wear properties, J. Manuf. Process. 59 (2020) 131–152, https://doi.org/10.1016/J.JMAPRO.2020.09.010.
[3] D.J. Lloyd, Particle reinforced aluminium and magnesium matrix composites, Int. Mater. Rev. 39 (1994) 1–23, https://doi.org/10.1179/imr.1994.39.1.1.
[4] B. Kaveendran, G.S. Wang, L.J. Huang, L. Geng, H.X. Peng, In situ (Al3Zr + Al2O3np)/2024Al metal matrix composite with novel reinforcement distributions fabricated by reaction hot pressing, J. Alloys Compd. 581 (2013) 16–22, https://doi.org/10.1016/j.jallcom.2013.06.143.
[5] R.A. Varin, Intermetallic-reinforced light-metal matrix in-situ composites, Metall. Mater. Trans. A 33 (2002) 193–201, https://doi.org/10.1007/S11661-002-0018-4, 2002 331.
[6] I. Dinaharan, G. Ashok Kumar, S.J. Vijay, N. Murugan, Development of Al3Ti and Al3Zr intermetallic particulate reinforced aluminum alloy AA6061 in situ composites using friction stir processing, Mater. Des. 63 (2014) 213–222, https://doi.org/10.1016/J.MATDES.2014.06.008.
[7] M. Balakrishnan, I. Dinaharan, R. Palanivel, R. Sathiskumar, Influence of friction stir processing on microstructure and tensile behavior of AA6061/Al3Zr cast aluminum matrix composites, J. Manuf. Process. 38 (2019) 148–157, https://doi.org/10.1016/J.JMAPRO.2018.12.039.
[8] G. Ashok Kumar, I. Dinaharan, S.J. Vijay, N. Murugan, Friction stir processing of intermetallic particulate reinforced aluminum matrix composite, Int. Assoc. Adv. Mater. 4 (2013) 230–234, https://doi.org/10.5185/AMLETT.2012.7398.
[9] J. McGinty, N. Yazdanpanah, C. Price, J.H. ter Horst, J. Sefcik, CHAPTER 1 nucleation and crystal growth in continuous crystallization, in: Handb. Contin. Cryst., Royal Society of Chemistry, 2020, pp. 1–50, https://doi.org/10.1039/9781788013581-00001.
[10] G.I. Eskin, D.G. Eskin, Ultrasonic Treatment of Light Alloy Melts, second ed., CRC Press, Boca Raton, Florida, USA, 2017.
[11] D.G. Eskin, I. Tzanakis, F. Wang, G.S.B. Lebon, T. Subroto, K. Pericleous, J. Mi, Fundamental studies of ultrasonic melt processing, Ultrason. Sonochem. 52 (2019) 455–467, https://doi.org/10.1016/J.ULTSONCH.2018.12.028.
[12] T.V. Atamanenko, D.G. Eskin, L. Zhang, L. Katgerman, Criteria of grain refinement induced by ultrasonic melt treatment of aluminum alloys containing Zr and Ti, Metall. Mater. Trans. 41 (2010) 2056–2066, https://doi.org/10.1007/s11661-010-0232-4.
[13] F. Wang, D. Eskin, J. Mi, C. Wang, B. Koe, A. King, C. Reinhard, T. Connolley, A synchrotron X-radiography study of the fragmentation and refinement of primary intermetallic particles in an Al-35 Cu alloy induced by ultrasonic melt processing, Acta Mater. 141 (2017) 142–153, https://doi.org/10.1016/j.actamat.2017.09.010.
[14] I. Tzanakis, G.S.B. Lebon, D.G. Eskin, K. Pericleous, Investigation of the factors influencing cavitation intensity during the ultrasonic treatment of molten aluminium, Mater. Des. 90 (2016) 979–983, https://doi.org/10.1016/j.matdes.2015.11.010.
[15] I. Tzanakis, G.S.B. Lebon, D.G. Eskin, K.A. Pericleous, Characterisation of the ultrasonic acoustic spectrum and pressure field in aluminium melt with an advanced cavitometer, J. Mater. Process. Technol. 229 (2016) 582–586, https://doi.org/10.1016/j.jmatprotec.2015.10.009.
[16] F. Wang, D. Eskin, J. Mi, T. Connolley, J. Lindsay, M. Mounib, A refining mechanism of primary Al3Ti intermetallic particles by ultrasonic treatment in the liquid state, Acta Mater. 116 (2016) 354–363, https://doi.org/10.1016/j.actamat.2016.06.056.
[17] A. Priyadarshi, M. Khavari, T. Subroto, M. Conte, P. Prentice, K. Pericleous, D. Eskin, J. Durodola, I. Tzanakis, On the governing fragmentation mechanism of primary intermetallics by induced cavitation, Ultrason. Sonochem. 70 (2021), 105260, https://doi.org/10.1016/j.ultsonch.2020.105260.
[18] A. Priyadarshi, M. Khavari, S. Bin Shahrani, T. Subroto, L.A. Yusuf, M. Conte, P. Prentice, K. Pericleous, D. Eskin, I. Tzanakis, In-situ observations and acoustic measurements upon fragmentation of free-floating intermetallics under ultrasonic cavitation in water, Ultrason. Sonochem. 80 (2021), 105820, https://doi.org/10.1016/J.ULTSONCH.2021.105820.
[19] F. Wang, I. Tzanakis, D. Eskin, J. Mi, T. Connolley, In situ observation of ultrasonic cavitation-induced fragmentation of the primary crystals formed in Al alloys, Ultrason. Sonochem. 39 (2017) 66–76, https://doi.org/10.1016/j.ultsonch.2017.03.057.
[20] W.C. Oliver, G.M. Pharr, Measurement of hardness and elastic modulus by instrumented indentation: advances in understanding and refinements to methodology, J. Mater. Res. 19 (2004) 3–20, https://doi.org/10.1557/jmr.2004.19.1.3.
[21] C.A. Schuh, Nanoindentation studies of materials, Mater. Today 9 (2006) 32–40, https://doi.org/10.1016/S1369-7021(06)71495-X.
[22] W.C. Oliver, G.M. Pharr, An improved technique for determining hardness and elastic modulus using load and displacement sensing indentation experiments, J. Mater. Res. 7 (1992) 1564–1583, https://doi.org/10.1557/JMR.1992.1564.
[23] M. Nakamura, K. Kimura, Elastic constants of TiAl3 and ZrAl3 single crystals, J. Mater. Sci. 26 (1991) 2208–2214, https://doi.org/10.1007/BF00549190.
[24] R.L. Fleischer, R.S. Gilmore, R.J. Zabala, Elastic moduli of polycrystalline, high-temperature binary intermetallic compounds, Acta Metall. 37 (1989) 2801–2803, https://doi.org/10.1016/0001-6160(89)90314-3.
[25] R.L. Fleischer, R.J. Zabala, Mechanical properties of diverse binary high-temperature intermetallic compounds, Metall. Trans. A 21 (1990) 2709–2715, https://doi.org/10.1007/BF02646066.
[26] J. Wang, S.L. Shang, Y. Wang, Z.G. Mei, Y.F. Liang, Y. Du, Z.-K. Liu, First-principles calculations of binary Al compounds: enthalpies of formation and elastic properties, Calphad 35 (2011) 562–573, https://doi.org/10.1016/J.CALPHAD.2011.09.009.
[27] L. Fu, J.L. Ke, Q. Zhang, B.Y. Tang, L.M. Peng, W.J. Ding, Mechanical properties of L12 type Al3X (X=Mg, Sc, Zr) from first-principles study, Phys. Status Solidi Basic Res. 249 (2012) 1510–1516, https://doi.org/10.1002/pssb.201248011.
[28] H. Hu, M. Zhao, X. Wu, Z. Jia, R. Wang, W. Li, Q. Liu, The structural stability, mechanical properties and stacking fault energy of Al3Zr precipitates in Al-Cu-Zr alloys: HRTEM observations and first-principles calculations, J. Alloys Compd. 681 (2016) 96–108, https://doi.org/10.1016/J.JALLCOM.2016.04.178.
[29] C. Li, N. Cheng, Z. Chen, Z. Xie, L. Hui, Intermetallic growth and interfacial properties of the grain refiners in Al alloys, Materials 11 (2018) 636, https://doi.org/10.3390/ma11040636.
[30] C.M. Li, S.M. Zeng, Z.Q. Chen, N.P. Cheng, T.X. Chen, First-principles calculations of elastic and thermodynamic properties of the four main intermetallic phases in Al-Zn-Mg-Cu alloys, Comput. Mater. Sci. 93 (2014) 210–220, https://doi.org/10.1016/j.commatsci.2014.06.031.
[31] G. Ghosh, A. van de Walle, M. Asta, First-principles calculations of the structural and thermodynamic properties of bcc, fcc and hcp solid solutions in the Al-TM (TM = Ti, Zr and Hf) systems: a comparison of cluster expansion and supercell methods, Acta Mater. 56 (2008) 3202–3221, https://doi.org/10.1016/j.actamat.2008.03.006.
[32] E. Clouet, J.M. Sanchez, C. Sigli, First-principles study of the solubility of Zr in Al, Phys. Rev. B Condens. Matter 65 (2002) 1–13, https://doi.org/10.1103/PhysRevB.65.094105.
[33] M. Conte, G. Mohanty, J.J. Schwiedrzik, J.M. Wheeler, B. Bellaton, J. Michler, N. X. Randall, Novel high temperature vacuum nanoindentation system with active surface referencing and non-contact heating for measurements up to 800 °C, Rev. Sci. Instrum. 90 (2019), 045105, https://doi.org/10.1063/1.5029873.
[34] A. Priyadarshi, T. Subroto, M. Conte, K. Pericelous, D. Eskin, P. Prentice, I. Tzanakis, Nanoindentation and cavitation-induced fragmentation study of primary Al3Zr intermetallics formed in Al alloys, in: Light Met. 2020, Springer, 2020, pp. 168–173, https://doi.org/10.1007/978-3-030-36408-3_23.
[35] C. Beckwith, G. Djambazov, K. Pericleous, T. Subroto, D.G. Eskin, D. Roberts, I. Skalicky, I. Tzanakis, Multiphysics modelling of ultrasonic melt treatment in the hot-top and launder during direct-chill casting: path to indirect microstructure simulation, Metals 11 (2021) 674, https://doi.org/10.3390/met11050674.
[36] S. Lu, B. Zhang, X. Li, J. Zhao, M. Zaiser, H. Fan, X. Zhang, Grain boundary effect on nanoindentation: a multiscale discrete dislocation dynamics model, J. Mech. Phys. Solid. 126 (2019) 117–135, https://doi.org/10.1016/J.JMPS.2019.02.003.

[37] T.B. Britton, D. Randman, A.J. Wilkinson, Nanoindentation study of slip transfer phenomenon at grain boundaries, J. Mater. Res. 24 (2009) 607–615, https://doi.org/10.1557/JMR.2009.0088, 2009 243.
[38] S. Zhen, G.J. Davies, Observations of the growth morphology of the intermetallic compound Al3Zr, J. Cryst. Growth 64 (1983) 407–410, https://doi.org/10.1016/0022-0248(83)90154-9.
[39] L. Li, Y. Zhang, C. Esling, K. Qin, Z. Zhao, Y. Zuo, J. Cui, A microstructural and crystallographic investigation of the precipitation behaviour of a primary Al3Zr phase under a high magnetic field, J. Appl. Crystallogr. 46 (2013) 421–429, https://doi.org/10.1107/S0021889813001258.
[40] J. Yanagimoto, Deformation (dislocations), in: CIRP Encycl. Prod. Eng., Springer, Berlin, Heidelberg, 2016, pp. 1–7, https://doi.org/10.1007/978-3-642-35950-7_6503-3.
[41] G. Yang, S.J. Park, Deformation of single crystals, polycrystalline materials, and thin films: a review, Materials 12 (2019) 2003, https://doi.org/10.3390/MA12122003, 12 (2019) 2003.
[42] X. Bi, X. Hu, Q. Li, Effect of Co addition into Ni film on shear strength of solder/Ni/Cu system: experimental and theoretical investigations, Mater. Sci. Eng. 788 (2020), 139589, https://doi.org/10.1016/J.MSEA.2020.139589.
[43] G. Zhang, F. Sun, H. Liu, X. Ren, H. Xu, M. Wang, Y. Fu, Exploration of d022-type Al3TM(TM = Sc, Ti, V, Zr, Nb, Hf, Ta): elastic anisotropy, electronic structures, work function and experimental design, Materials 14 (2021) 2206, https://doi.org/10.3390/MA14092206.
[44] C.L. Chen, A. Richter, R.C. Thomson, Mechanical properties of intermetallic phases in multi-component Al–Si alloys using nanoindentation, Intermetallics 17 (2009) 634–641, https://doi.org/10.1016/J.INTERMET.2009.02.003.
[45] Y.Ö. Çiftci, K. Çolakoğlu, C. Çoban, E. Deligöz, The structural, elastic and thermodynamic properties of intermetallic compound CeGa2, Cent. Eur. J. Phys. 10 (2012) 197–205, https://doi.org/10.2478/S11534-011-0012-9/MACHINEREADABLECITATION/RIS.
[46] A. Barnoush, Correlation between dislocation density and nanomechanical response during nanoindentation, Acta Mater. 60 (2012) 1268–1277, https://doi.org/10.1016/J.ACTAMAT.2011.11.034.
[47] B. Bor, D. Giuntini, B. Domènech, M.V. Swain, G.A. Schneider, Nanoindentation-based study of the mechanical behavior of bulk supercrystalline ceramic-organic nanocomposites, J. Eur. Ceram. Soc. 39 (2019) 3247–3256, https://doi.org/10.1016/J.JEURCERAMSOC.2019.03.053.
[48] S. Pathak, J.L. Riesterer, S.R. Kalidindi, J. Michler, Understanding pop-ins in spherical nanoindentation, Appl. Phys. Lett. 105 (2014), 161913, https://doi.org/10.1063/1.4898698.
[49] J.D. Kiely, R.Q. Hwang, J.E. Houston, Effect of surface steps on the plastic threshold in nanoindentation, Phys. Rev. Lett. 81 (1998) 4424, https://doi.org/10.1103/PhysRevLett.81.4424.
[50] J.A. Zimmerman, C.L. Kelchner, P.A. Klein, J.C. Hamilton, S.M. Foiles, Surface step effects on nanoindentation, Phys. Rev. Lett. 87 (2001), 165507, https://doi.org/10.1103/PhysRevLett.87.165507.
[51] F. Pöhl, Pop-in behavior and elastic-to-plastic transition of polycrystalline pure iron during sharp nanoindentation, Sci. Rep. 9 (2019) 1–12, https://doi.org/10.1038/s41598-019-51644-5.
[52] G. L'Hôte, S. Cazottes, J. Lachambre, M. Montagnat, P. Courtois, J. Weiss, S. Deschanel, Dislocation dynamics during cyclic loading in copper single crystal, Materialia 8 (2019), 100501, https://doi.org/10.1016/J.MTLA.2019.100501.
[53] B. Wolf, A. Richter, The concept of differential hardness in depth sensingindentation, New J. Phys. 5 (2003) 15, https://doi.org/10.1088/1367-2630/5/1/315.
[54] I. Tzanakis, D.G. Eskin, A. Georgoulas, D.K. Fytanidis, Incubation pit analysis and calculation of the hydrodynamic impact pressure from the implosion of an acoustic cavitation bubble, Ultrason. Sonochem. 21 (2014) 866–878, https://doi.org/10.1016/j.ultsonch.2013.10.003.
[55] M. Khavari, A. Priyadarshi, A. Hurrell, K. Pericleous, D. Eskin, I. Tzanakis, Characterization of shock waves in power ultrasound, J. Fluid Mech. 915 (2021), https://doi.org/10.1017/jfm.2021.186. R3.
[56] C.L. Chen, A. Richter, R.C. Thomson, Investigation of mechanical properties of intermetallic phases in multi-component Al–Si alloys using hot-stage nanoindentation, Intermetallics 18 (2010) 499–508, https://doi.org/10.1016/J.INTERMET.2009.09.013.
[57] A. Richter, C.L. Chen, R. Smith, E. McGee, R.C. Thomson, S.D. Kenny, Hot stage nanoindentation in multi-component Al–Ni–Si alloys: experiment and simulation, Mater. Sci. Eng. 494 (2008) 367–379, https://doi.org/10.1016/J.MSEA.2008.04.057.
[58] R. Gupta, B.S.S. Daniel, Impression creep behaviour of ultrasonically processed in-situ Al3Zr-Al alloy composite in as-cast condition, Mater. Char. 169 (2020), 110594, https://doi.org/10.1016/J.MATCHAR.2020.110594.
[59] J. Xia, C.X. Li, H. Dong, Hot-stage nano-characterisations of an iron aluminide, Mater. Sci. Eng. 354 (2003) 112–120, https://doi.org/10.1016/S0921-5093(02)00902-4.
[60] J. Musil, F. Kunc, H. Zeman, H. Poláková, Relationships between hardness, Young's modulus and elastic recovery in hard nanocomposite coatings, Surf. Coating. Technol. 154 (2002) 304–313, https://doi.org/10.1016/S0257-8972(01)01714-5.
[61] Y.T. Cheng, C.M. Cheng, Scaling, dimensional analysis, and indentation measurements, Mater. Sci. Eng. R Rep. 44 (2004) 91–149, https://doi.org/10.1016/J.MSER.2004.05.001.